ELSEVIER

NeuroImage

www.elsevier.com/locate/ynimg
NeuroImage 29 (2006) 879 – 887

Combined imaging–histological study of cortical laminar specificity of fMRI signals

Noam Harel,* Joseph Lin, Steen Moeller, Kamil Ugurbil, and Essa Yacoub

Center for Magnetic Resonance Research, Department of Radiology, University of Minnesota Medical School, 2021 6th Street SE Minneapolis, MN 55455, USA

Received 30 March 2005; revised 22 June 2005; accepted 11 August 2005
Available online 27 September 2005

Since the commencement of functional magnetic resonance imaging (fMRI), great effort has been put into increasing its spatial resolution and signal specificity from vessel-weighted to more tissue-specific signals. The working assumption is that the "tissue" signals closely mirror changes at the neuronal level. While great progress has been made, the basic and most fundamental questions remain unanswered: where in the gray matter do these "tissue fMRI" changes occur?

Recently, the temporal correspondence of hemodynamic-based fMRI signals and neurophysiological activity was explored. The data suggest, although not conclusively, that the local field potential (LFP) response gives a better estimate of changes that accompany increased neuronal activity. LFP are thought to be generated by synaptic activity reflecting input signals into layer IV within a cortical region. If so, the spatial distribution of the fMRI signal should be specific to the corresponding cortical lamina.

Here, in a combined imaging and histological study, the spatial characteristics of fMRI signals across the lamina were explored. In a high-resolution fMRI study ($0.15 \times 0.15 \times 2$ mm^3), the spatial specificity of fMRI signals was correlated with the underlying cortical laminar cytoarchitectonic obtained within the same animal and tissue region. We demonstrate that when surface vessels are excluded high-resolution fMRI signals peak at cortical layer IV.

Introduction

Functional magnetic resonance imaging (fMRI; Kwong et al., 1992; Ogawa et al., 1992) has significantly increased our knowledge of brain function and the neural basis of human cognition. The methodology is based on detecting MRI signal alterations which reflect changes in cerebral blood flow, blood volume and oxygen consumption rate. Since its introduction, blood-oxygen-level-dependent (BOLD; Ogawa et al., 1990) fMRI has emerged as one of the most commonly employed methodologies for studying brain function. As a result, great effort has been put into better understanding of its neuronal correlations with the goal of increasing the spatio-temporal resolution and specificity of these hemodynamic-based signals (Ugurbil et al., 2003). These efforts focused predominantly on suppressing draining vessel contributions and boosting tissue or capillary signals (Duong et al., 2001; Yacoub et al., 2003), all with the assumption that gray matter or "tissue"-fMRI signals closely mirror changes at the neuronal level.

A quantitative relationship between the BOLD signal and spiking activity was explored by several groups, suggesting a linear correlation (Heeger et al., 2000; Ress et al., 2000). More recently, the temporal correspondence between these hemodynamic signals and neurophysiological activity was explored. Based on concurrent measurements of single- and multi-unit recordings with either BOLD fMRI signals in the monkey visual cortex (Logothetis et al., 2001) or cerebral blood flow (the most dominant contributor to BOLD signals) in rat cerebellum (Mathiesen et al., 1998), the local field potential (LFP) response rather than spiking activity is thought to give better estimates of the physiologic and metabolic changes that accompany increased neuronal activity.

In cerebral cortex, the laminar distribution of neurons gives rise to six anatomically and functionally distinct layers, numbered sequentially from the surface to the white matter. Each layer receives input from, and projects to, distinct locations. For example, in primary visual cortex, layer IV is the main input layer from the thalamic nuclei; upper layers project mainly forward to higher order visual areas, while deeper layers project mainly backwards to subcortical structures. Thus, based on the functional neurophysiological findings (Mathiesen et al., 1998; Logothetis et al., 2001), the spatial distribution of fMRI signals should be specific to the foci of the input layers. However, the spatial correspondence of the fMRI signals and the anatomical configuration has never been concurrently investigated at the cortical laminar level.

Here, in a combined imaging and histological study, we demonstrate that high-resolution tissue fMRI signals peak at cortical layer IV.

* Corresponding author. Fax: +1 612 626 2004.
E-mail address: noam@cmrr.umn.edu (N. Harel).
Available online on ScienceDirect (www.sciencedirect.com).

1053-8119/$ - see front matter © 2005 Elsevier Inc. All rights reserved.
doi:10.1016/j.neuroimage.2005.08.016

Materials and methods

Animal preparation

Cats ($n = 3$) were prepared as described previously (Harel et al., 2002). The animals were kept under isoflurane anesthesia throughout the experiment (1% in a N_2O:O_2 mixture of 70:30). Blood pressure, end-tidal CO_2 and body temperature were maintained at normal conditions. Visual stimuli consisted of binocular 40-s high-contrast square-wave moving gratings (0.15 cyc/degree, 2 cyc/s). All MR experiments were performed on a 9.4 T/31 cm magnet (Oxford, UK) equipped with a console by Varian Inc., (Palo Alto, CA, USA).

Coils and slice selection

To maximize signal sensitivity, two different coils were used. For the fMRI study, a small (ID 1.4 cm) transmit and receive coil with high sensitivity was used. For the 3D anatomical images, where more uniform excitation profiles are needed, a larger coil was used. The coils were uncoupled and driven independently.

A single coronal slice perpendicular to area 18 (crossing at Horsley-Clark AP2) was used for the functional study. To adequately resolve fMRI signals across the tissue, high in-plan resolution was needed (see below). Due to SNR limitations, a 2 mm slice thickness was used. To minimize partial volume effects in the image plane, the functional slice was chosen in a relatively flat section of area 18, having a comparatively uniform representation of the cortical layers within the imaged plane. Anatomic images were obtained using T_1-weighted 2D TurboFLASH and a T_1-weighted 3D gradient echo multi-slice (GEMS) sequence with a matrix size of $128 \times 128 \times 128$ over a field of view of $5 \times 5 \times 5$ cm^3.

Functional MRI parameters

Two contrast mechanisms were used for the functional studies: BOLD and CBV-weighted signals. In addition, two imaging sequences were used, Gradient Echo (GE) and Hahn Spin Echo (HSE). Initially, GE- and HSE-BOLD contrast responses were measured. Next, CBV-weighted changes were measured following a bolus injection of monocrystalline iron oxide nanoparticles (MION) (Kennan et al., 1998; Mandeville et al., 1998) (10 mg Fe/kg) using a GE EPI acquisition. Image parameters for the GE were: data matrix = 128×128, 4 segment EPI, field of view (FOV) = 1.92×1.92 cm^2. Slice thickness = 2 mm and TE/TR = 20 ms (10 ms with MION)/1 s. The scan time for 1 image (4 segments) was 4 s. The flip angle used was 60° corresponding to the Ernst angle. For the HSE EPI sequence, a reduced FOV along the phase encode direction was applied using a selective refocusing pulse. This allowed us to reduce the number of segments needed for the high-resolution images. Imaging parameters: FOV: 3.84×0.96 cm^2 (matrix 256×64); slice thickness = 2 mm; 2 segments. TE/TR = 40 ms/2 s. The scan time for 1 image was 4 s. Both image sequences yielded an in-plane resolution of 0.15×0.15 mm^2 without any zero filling. The EPI readout time at this spatial resolution was 0.7 ms for a single line of k-space. Both GE- and HSE-weighted acquisitions had 32 readout lines per segment, yielding a total readout time of 22.4 ms, thus the spatial blurring due to the EPI readout is negligible (Haacke et al., 1999).

Functional MRI data processing was performed with the Stimulate software (Strupp, 1996) and a home written Matlab code (The MathWorks, Inc.). No temporal or spatial smoothing was applied. The MR signals were cross-correlated with the stimulation paradigm to identify active pixels using an ideal boxcar function that emulated the stimulus protocol (Bandettini et al., 1993).

Data analysis

Signal profiles were generated by plotting averaged multiple lines (typically $7 \approx 1$ mm) across the dorsal segment of the marginal gyrus (area 18; see also Fig. 3e). This region was chosen for several reasons; the visual stimulus was optimized to elicit responses from neurons in area 18 (Movshon et al., 1978); the close proximity to the coil allowed higher sensitivity, and the region has relatively uniform curvature.

To determine whether signal changes at layer IV were statistically different from neighboring layers, a t test was computed between layer IV and layers I, II/III and the infragranular layers combined (layers V and IV) (Table 1). For quantification analysis, the data from the 3 cats were pooled. To align the spatial distribution of signal changes from different cats with different lamina widths, signal change profiles were resampled non-linearly to exhibit an equal number of samples in each cortical layer based on a reference (cat #2). To maintain an unbiased resampling, a linear interpolation was used to estimate intermediate values. To quantify the signal changes as a function of cortical lamina between animals, a normalization process was done. Since the absolute MR signal level heavily depends on instrumental factors such as coil position and gain, as well as on physiological factors, such as mean blood pressure, the absolute signal changes were converted to express the ratio of signal change at each of the layers (I, II/III, V and IV) relative to the signal change at layer IV (e.g., layer I/layer IV), within each animal and are summarized in Table 2. Error bars in Fig. 5 indicate one standard deviation.

Co-registration of MRI and histology

The co-registration of the MR images with the histology preparation was achieved manually by a multi-stage aligning process. Initially, the 3D GEMS volume was loaded into

Table 1
Statistical significance differences in signal amplitudes

P values	Cat 1			Cat 2			Cat 3			Averaged ($n = 3$)		
	I	II/III	V/VI	I	II/III	V/VI	I	II/III	V/VI	I	II/III	V/VI
GE-BOLD	<0.001	0.913	0.005	<0.001	0.044	<0.001	<0.001	<0.001	0.039	<0.001	0.003	0.004
HSE-BOLD	0.016	<0.001	<0.001	0.009	0.09	<0.001	0.737	0.04	0.005	0.066	<0.001	0.001
CBV-weighted	0.109	0.181	<0.001	<0.001	0.669	<0.001	<0.001	0.278	<0.001	<0.001	0.841	<0.001

To determine whether signal changes at layer IV were statistically different from neighboring layers, a t test was computed between layers IV and layers I, II/III and layers V and IV, respectively. Averaged data are shown in the right column (see Materials and methods). Values represent P values.

Table 2
Relative signal changes as a function of cortical lamina

Ratios	Cat 1				Cat 2				Cat 3				Averaged			
	I	II/III	V	VI	I	II/III	V	VI	I	II/III	V	VI	I	II/III	V	VI
GE-BOLD	2.75	1.24	1.04	0.85	1.46	0.96	0.68	0.71	2.03	1.81	0.82	0.78	2.08	1.34	0.85	0.78
HSE-BOLD	0.72	0.68	0.90	0.78	0.75	0.34	0.74	0.67	0.71	0.77	0.8	0.71	0.73	0.60	0.81	0.72
CBV-weighted	0.83	1.01	0.81	0.70	0.75	1.03	0.59	0.37	0.20	0.82	0.61	0.46	0.59	0.96	0.67	0.51

To compare between animals and compensate for different baseline signal levels, the absolute MR signal changes in each layer were converted to the ratio of signal amplitude changes between layers I, II/III, V and VI relative to signal changes in layer IV.

BrainVoyager (BrainInnovation, Netherlands). The 3D coronal image (Fig. 1) was matched with the T_1-weighted EPI image of the functional slice (e.g., see also Fig. 4b). Multiple visible anatomical landmarks were used in this stage such as the shape, curvature and orientation of the marginal gyrus; shape and orientation of the white matter innervating across the tissue; shape and curvature of the cingular sulcus; shape and depth of the lateral sulcus; and the shape and width of the corpus callosum.

The 3D volume was then resliced with a dorsal view (transversal plane) while keeping the location of the coronal slice (A–P axis) marked. Thus, the location of the coronal functional plane was indicated on the cortical surface (Fig. 1, bottom left). A set of digital photographs of the intact brain was taken with a dorsal view (Fig. 2). Then, the MR image in the transverse plane (Fig. 2a) was aligned with a photographed dorsal view of the intact brain (Fig. 2b); visible anatomical landmarks such as the midline, sulci and imprints of large surface vessels which appear in the MR image were used (Adobe Photoshop). Once the image plane was determined (Fig. 2c), a 3 mm cortical slab was sectioned, and the block underwent histological preparation. The accuracy of the matching technique, in the A–P axis, is at most 2 mm corresponding to the slice thickness of the EPI images. Thus, the functional slice was chosen to be in a relatively flat section of area 18, minimizing the cytoarchitectonic variance within the image.

Histology

Following the MR session, the animals were transcardially perfused with 0.1 M phosphate-buffered saline followed by a 4% paraformaldehyde (PA) in 0.1 M phosphate buffer. The brain was removed and was postfixed in 4% PA. Digital photographs were taken of the intact fixed brain. A 3 mm cortical slab (see above) was extracted. The cortical slab was then sectioned with a 15 μm slice thickness with a cryostat and stained with cresyl violet (Nissl).

Figs. 3a and b show a high-resolution T_1-weighted image of the slice used for all functional studies and a low-magnification

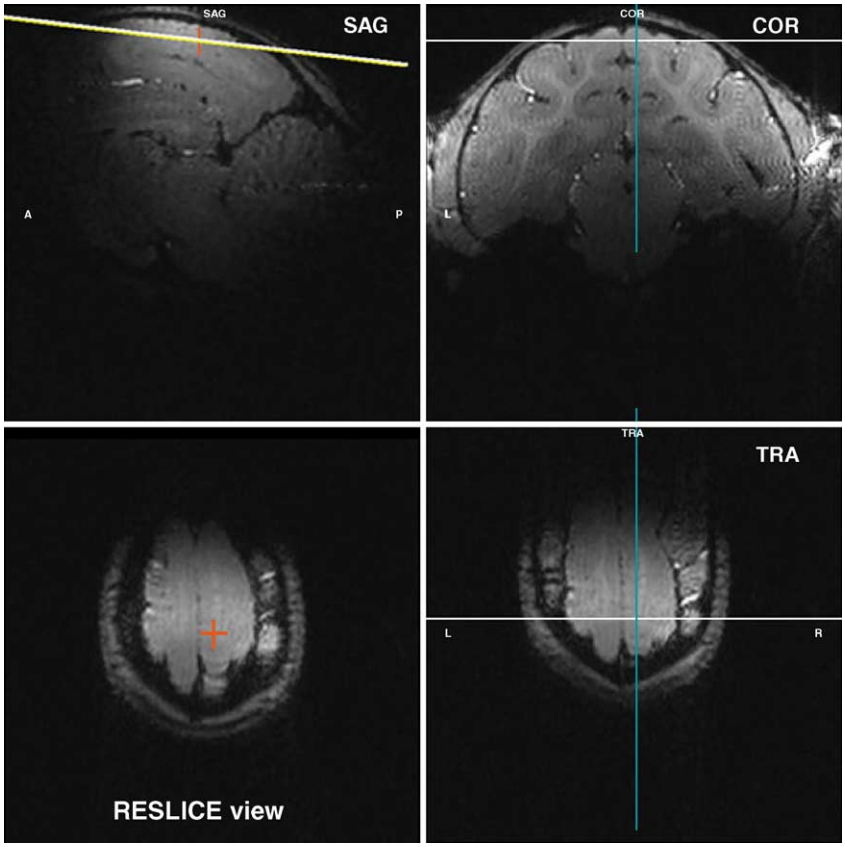

Fig. 1. Slice selection. A 3D volume of the cat's brain is displayed in 3 planes: sagittal (SAG), coronal (COR) and transverse (TRA). The coronal slice (top right) corresponds to the slice used in the functional studies. A dorsal view of the brain marked with the functional slice (lower left).

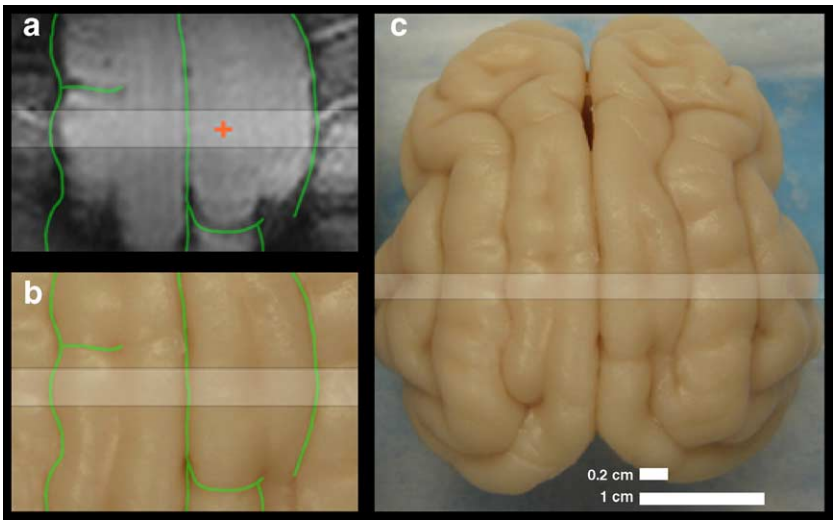

Fig. 2. Alignment of MR image with the intact brain. A dorsal view MR image with the marked functional slice (a) is aligned with a digital photographed dorsal view of the intact brain (b). Visible anatomical landmarks are indicated (green lines). Once the two images are aligned, the location of the coronal slice is superimposed (horizontal line) on the full view photograph of the brain (c) and is used as a blueprint for sectioning and extracting the corresponding cortical slab.

photograph of the corresponding Nissl stain, respectively. Note the high resemblance between the two images. To identify and classify cells, the histologically stained slices were viewed with a microscope (Olympus BX60). Figs. 3c and d are two examples of higher magnification images taken from the regions that the fMRI signals were recorded. The cortical surface is indicated (Fig. 3c; top right). The lamination of the cortical tissue is essentially based on the disposition of cell bodies of various types, sizes and cell densities. To identify the border between layers, the histological slide was viewed under a high-power magnification. The first clear observation is an area which is only lightly stained. This region is layer I (Fig. 3c). Moving downward and deeper across the tissue, a sudden increase in cell density is observed (arrow). This is the border between layers I and II. Layer II is populated by small pyramidal cells that are concentrated at its upper border. With increasing depth, the small pyramidal cells gradually give way to larger ones. This progressive increase in the size and the more distributed nature of the neurons with depth continue into layer III, however, there is no distinct boundary between layers II and III (O'Leary, 1941). The lower portion of layer III is characterized with large pyramidal cells with irregular-shaped cell bodies, "border pyramids", which demarcate the lower border with layer IV (arrow). In general, neurons in layer IV are small and more closely packed.

Another example is shown in Fig. 3d which was taken from a deeper section of the border between gray and white matter (WM). The neurons in layer VI tend to be arranged into vertical stacks and columns that are separated by clear spaces that do not contain staining afferents and efferent axons (left hand side in Fig. 3d). Layer V is more characterized by mid size pyramidal cells which are more sparse. Thus, by using the well-defined features of neuronal arrangements, we defined the boarder between cortical layers within the image plane.

Due to the high magnification used, a limited field of view is obtained. Therefore, to generate an image of the entire coronal slice, a series of multiple high magnification images were captured. Then, a mosaic of these individual frames was used to reconstruct one image (Fig. 3e). The outcome is an image of the histological-stained slice of primary visual cortex corresponding to the slice used for the fMRI study (Fig. 3e; outlined in Fig. 3b). The borders between the layers are superimposed (Fig. 3e; white lines). Thus, we obtained the anatomically defined borders between cortical layers within our imaged plane.

One major concern when dealing with histological slides is the known problem of tissue shrinkage as a result of the dehydration process. However, tissue shrinkage occurs linearly (Schuz and Palm, 1989), thus, it does not affect the relative dimensions of the cortical layers.

Results

Utilizing a high magnetic field (9.4 Tesla (T)), we have acquired fMRI signals at ultra high resolution ($0.15 \times 0.15 \times 2$ mm^3) across cortical layers of the anesthetized cat visual cortex (Fig. 4). In addition, the corresponding cortical tissue underwent histological staining to anatomically define the laminar borders within the imaging plane. Thus, combined with different imaging contrasts, the spatial laminar origin of fMRI signals was investigated. In each study, BOLD contrast was measured using two different imaging sequences, the conventional T_2*-weighted Gradient Echo (GE) and the Hahn Spin Echo (HSE) T_2-weighted sequence which, at high magnetic fields, is expected to have better specificity to the microvasculature (i.e., capillary and smaller size venules) (Boxerman et al., 1995). Subsequently, cerebral blood volume (CBV)-weighted changes were measured following a bolus injection of monocrystalline iron oxide nanoparticles (MION) (Kennan et al., 1998; Mandeville et al., 1998), an exogenous MRI contrast agent with a long blood half life. A single coronal slice orthogonal to the cortical surface was used (Figs. 4a and b). In all three functional maps, spatially defined and localized signal changes were confined to the primary visual areas (Brodmann's areas 17 and 18; medial and dorsal parts of marginal gyrus, respectively) and followed closely the gray matter contour during a visual stimulation task consisting of 40 s of drifting bars (Figs. 4c–e). The activation patterns were not uniform across the cortical tissue. When the surface regions that contain large vessels were excluded, a strip of elevated signal changes centered over the

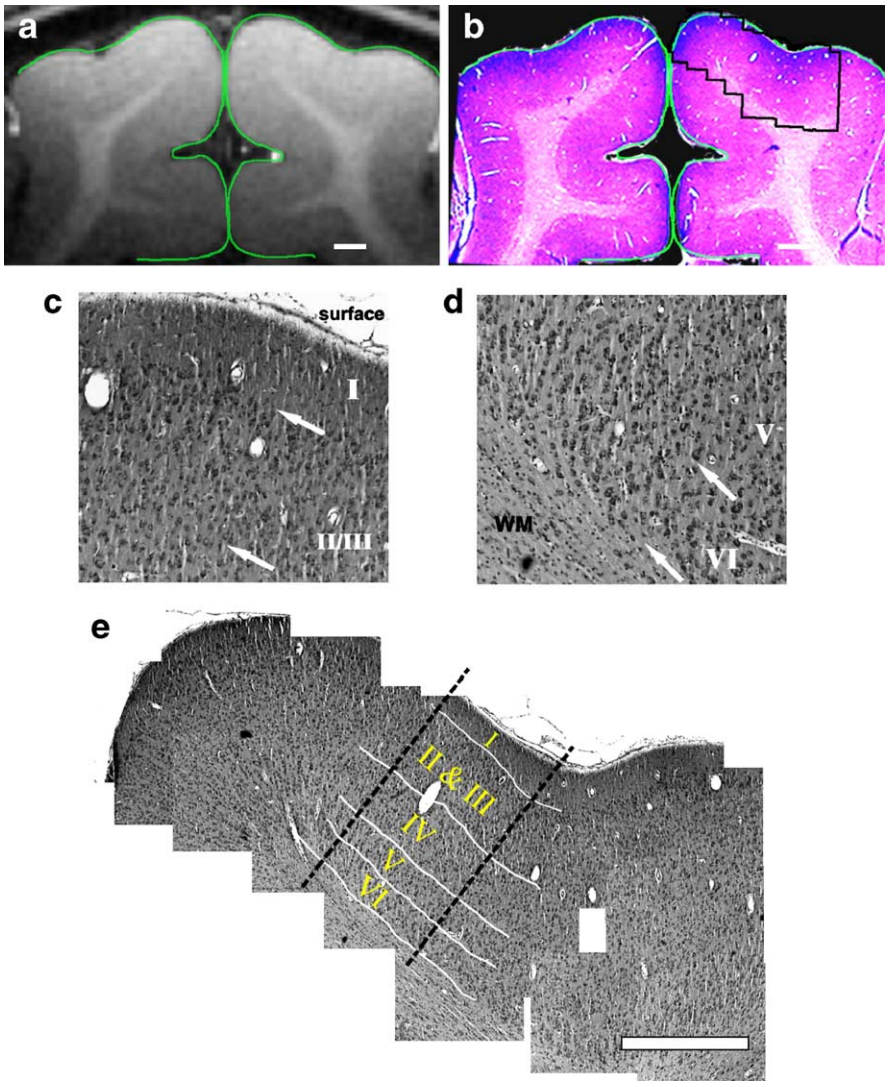

Fig. 3. Co-registration of MR image with the corresponding cortical tissue. Following the imaging session, the brain was removed, and the imaged slice was identified in the intact brain. (a) High-resolution T_1-weighted image of the slice used for all functional studies. (b) Low-magnification photograph of the corresponding Nissl stain (histology) of the same region. Note the high resemblance between the two images. (c and d) High-magnification photographs of cross sections across the gray matter in primary visual cortex. White arrows indicate borders between cortical lamina. (e) A mosaic reconstruction of high-magnified Nissl-stained images (right hemisphere) of cortical tissue corresponding to the imaged plane (outlined in panel b). White lines: the anatomically defined borders between cortical layers. Black lines: region used for plotting signal profiles (area 18). Scale bar = 1 mm. WM = white matter.

gray matter was observed in all maps, most pronounced in the CBV-weighted maps.

To determine the cortical laminar derivation of these peak tissue signals, we developed a method to identify and extract the cortical slab corresponding to the MR image plane so that the borders between the cortical layers in the imaged slice could be anatomically defined. In order to compare the histology data with the translaminar functional imaging signals, raw stimulus-evoked fMRI signal changes (ΔS) were plotted across the tissue as a function of cortical depth (Fig. 5); these ΔS plots were generated without applying any statistical threshold to classify the pixels as "activated" or not. The abscissas represent distance from the surface down to the white matter (see Materials and methods). The anatomically defined borders between the layers (e.g., as derived in Fig. 3e) were superimposed. To show the consistency of our findings, signal profiles from three cats, generated with similar analysis, are shown. In addition, the data from the 3 cats were normalized with respect to laminar distance and pooled together (see Materials and methods).

Spatial specificity of GE-BOLD signal

The largest GE-BOLD signal changes occurred mainly at the cortical surface presumably from superficial cortical vessels (Figs. 4c and 5 top row). The signal changes at the surface region/layer I, was more than double when compared to changes at layer IV and seemed to "spillover" into layer II/III. This observation is consistent with previous theoretical and experimental findings which indicate that GE-BOLD signals retain a non-specific component (i.e., draining vessels) even at high magnetic fields due to extravascular BOLD effects that fall in the static averaging (dephasing) domain (e.g., Ogawa et al., 1993). The GE-BOLD data must also contain signals originating from the microvasculature; although the microvascular contribution relative to larger vessels is

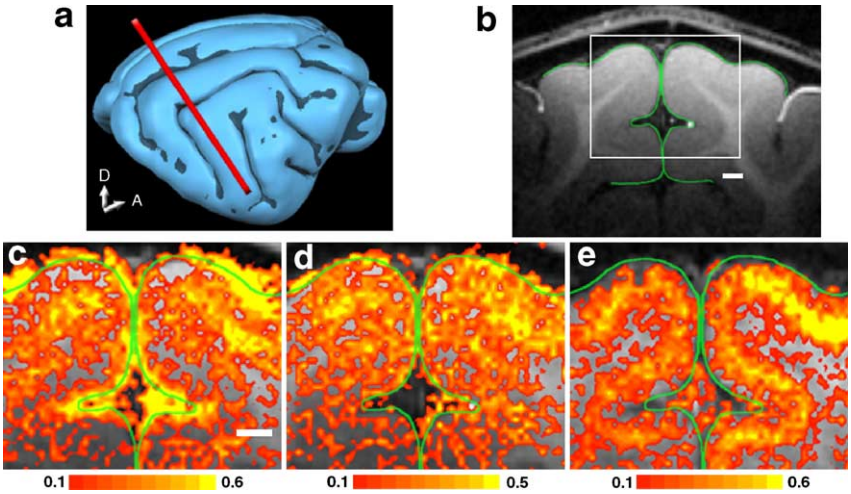

Fig. 4. High-resolution fMRI (0.15 × 0.15 mm^2 in-plane resolution). Cross correlation activation maps for a 40-s drifting bars stimuli. (a) A schematic illustration of the slice selection. (b) T_1-weighted coronal image across primary visual cortex. (c) Gradient Echo (GE) BOLD map; (d) Hahn Spin Echo (HSE) BOLD map; (e) contrast enhanced GE CBV-weighted (MION) maps. Signal changes were confined to the primary visual areas and closely followed the gray matter contour. In all three maps, a spatially defined band of elevated signal changes was centered over the gray matter. A: anterior; D: dorsal; Scale bar = 1 mm.

smaller in GE-BOLD, it increases approximately supra-linearly with the magnetic field (Ogawa et al., 1993; Yacoub et al., 2003). A localized increase in GE-BOLD signals was indeed observed over layer IV (Figs. 4c and 5 top row).

Spatial specificity of HSE-BOLD signal

When compared to GE-BOLD, HSE-BOLD is expected to have significantly better specificity at high magnetic fields (Duong et al., 2003; Yacoub et al., 2003, 2005), albeit at the cost of a decrease in the magnitude of stimulus-evoked signal changes. The improved specificity is ascribed to the enhanced sensitivity to the microvasculature via extravascular BOLD, while the potentially non-specific intravascular component rapidly diminishes with increasing field magnitude due to the shortening of the apparent T_2 of venous blood (Thulborn et al., 1982; Yacoub et al., 2001; Duong et al., 2003) compared to tissue. As suggested by earlier theoretical work, our HSE-BOLD functional maps exhibit reduced superficial large vessels signals when compared to GE-BOLD (factor of 2.8; Table 2) which dominate the GE-BOLD maps; more importantly, maximum signal changes in the tissue were observed in layer IV, a region dominated by microvascular size vessels (Figs. 4d and 5 middle raw). Even with the HSE sequence at high magnetic field (9.4 T), a measurable non-specific vessel signal change is present in the vicinity of the surface region. The source of these large vessels changes could be the result of experimental limitations that

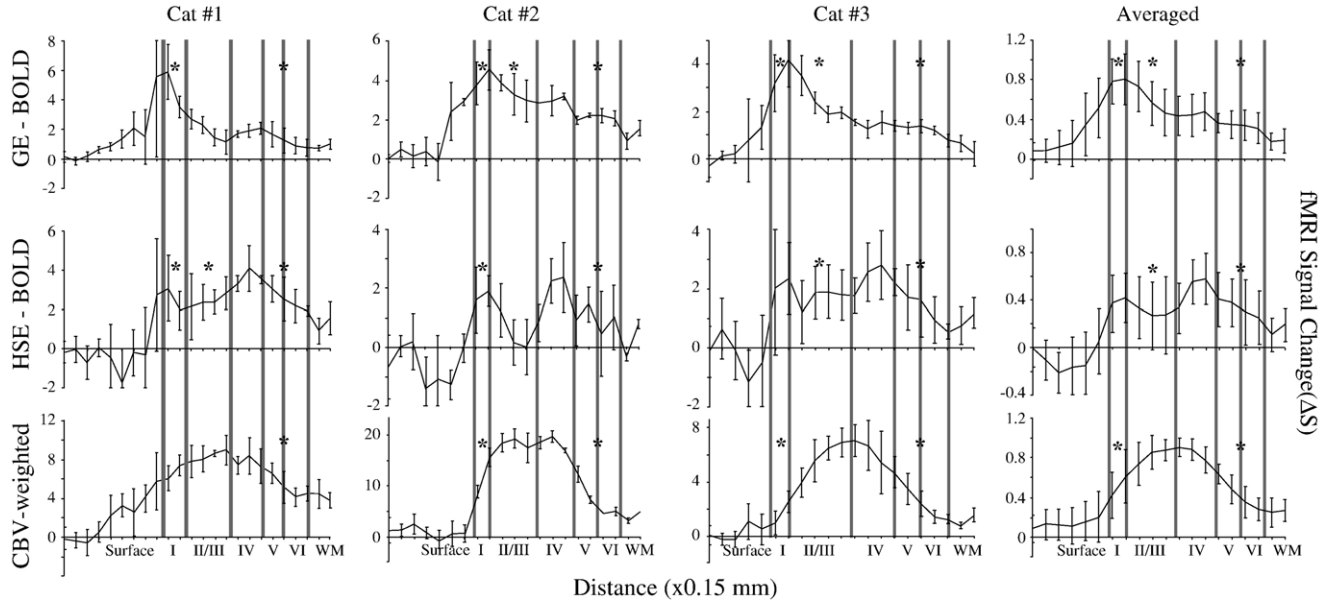

Fig. 5. fMRI signal changes as a function of cortical depth. Raw fMRI signal changes (ΔS), without applying any statistical threshold, were plotted across the tissue as a function of cortical depth. The abscissa represents distance from the surface down to the white matter. The anatomically defined borders between the layers are superimposed. To show the consistency of our findings, signal profiles from three cats are shown. Averaged data are shown in the right column (see Materials and methods). Error bars = 1 SD. *$P < 0.005$ compared to signal changes at layer IV.

result in less than ideal execution of the HSE contrast, leading to non-T_2 contributions, primarily due to either inflow effects (see Duong et al., 2003; Yacoub et al., 2003) or T_2' effects due to the EPI readout. While a clear difference exists in the upper layer region between the GE- and the HSE-BOLD signals, due to a higher sensitivity of the former to larger vessels, interestingly, the ratios between layer IV and deeper layers (V and IV) were similar (Table 2). This is anticipated due to the fact that in this region little or no large vessels are present.

Spatial specificity of CBV-weighted signal

Following the intravenous injection of MION, the MR signal diminishes because of the change in the magnetic susceptibility of vascular space and consequent generation of magnetic field inhomogeneities around blood vessels. Blood volume increases at a constant level of MION and induces further signal decreases in T_2*-weighted images (Kennan et al., 1998; Mandeville et al., 1998, 2004). Due to the enhanced sensitivity from the paramagnetic iron oxides used, overall stimulus-evoked signal changes (i.e., contrast-to-noise ratio (CNR)) at the tissue increased by a factor of ~4 when compared to BOLD at the echo times used in this study. During the visual task, maximum CBV changes were significantly higher and peaked at the deeper portion of layer III and extended down into layer IV (Fig. 5, lower row). Furthermore, CBV-weighted signal changes were broader than those of the BOLD signals over the middle layers, suggesting that there are differences in the mechanisms underlying each technique.

The stimulus used here was optimized for evoking responses from neurons in area 18; in contrast, the neurons in area 17 prefer higher spatial frequencies with slower velocities (Movshon et al., 1978). Fig. 6 demonstrates the corresponding spatial specificity of the CBV signals. The largest CBV changes correspond to area 18 (dorsal section of marginal gyrus) and seem to consistently mark the medial edge of area 18 into the transition zone (TZ) (Payne, 1990)—the region bordering between areas 18 and 17 (medial section of marginal gyrus).

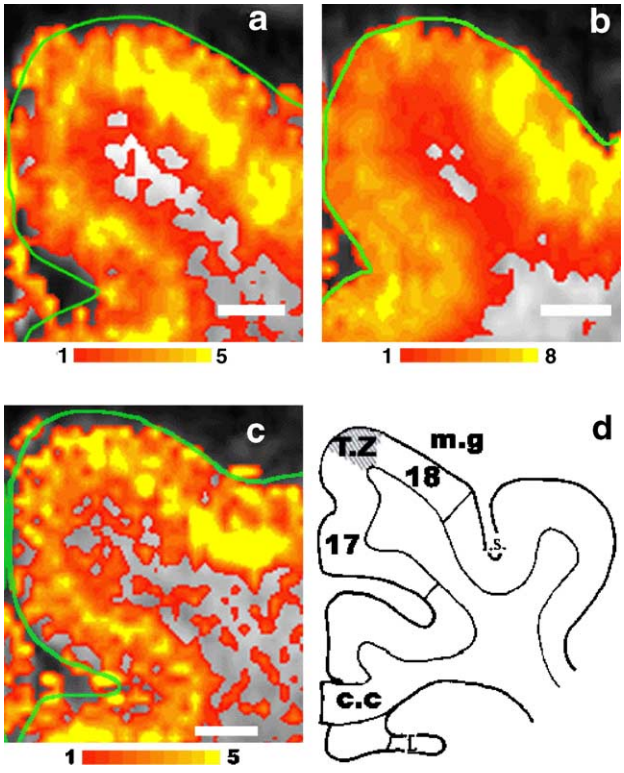

Fig. 6. Specificity of CBV-weighted signals. Under the experimental stimulus used, maximum CBV-weighted signal changes appear specific to area 18 (dorsal section of marginal gyrus) with a sharp drop in signal changes towards the transition zone (TZ) and area 17 (medial section of marginal gyrus). (a–c) CBV-weighted percent signal change activation maps (right hemisphere) from 3 cats. (d) An outline drawing of the cat's cerebral right hemisphere to show the positions of areas 17, 18 and the TZ (modified from Payne, 1990). m.g.: marginal gyrus; c.c: corpus callosum. Scale bar = 1 mm. Color bar = percent signal change.

Discussion

In this work, the laminar spatial specificity of tissue fMRI signals were investigated in a high-field, high-resolution fMRI study and correlated with postmortem histological-stained slices obtained within the same animal and tissue region. Tissue fMRI signal changes centered over layer IV were observed with three different fMRI contrast mechanisms when excluding the surface vessels region. This finding is in good agreement with previous cerebral blood flow (CBF) fMRI (Duong et al., 2000) and neurophysiological data (Caesar et al., 2003).

At high magnetic fields, GE-BOLD functional maps are expected to display contributions from large blood vessels, as at low magnetic fields, but also from the microvasculature (capillaries and post-capillary venules), whereas HSE-BOLD maps should be dominated by contribution from the capillaries. These mechanistic expectations, however, were inferred based on theoretical considerations (Boxerman et al., 1995), and magnetic field dependence of the stimulus induced signal changes for the two methods (Duong et al., 2003; Yacoub et al., 2003). The cat studies presented here confirm these expectations directly because of the spatially distinct distributions of the different parts of the vascular tree. It is well known that the capillaries are not evenly distributed across layers (Harrison et al., 2002) and that layer IV has the highest capillary density in cats (Pawlik et al., 1981). When the large vessel contamination from the cortical surface is excluded, the translaminal distributions of both the GE and HSE fMRI signals approximately reflect the capillary density in the different layers. The post-capillary venules that run perpendicular to the cortical surface must also contribute to both the HSE- and especially to the GE-BOLD effect; however, based on their orientation, these blood vessels most likely yield relatively uniform laminar fMRI signals as observed in area 17 (Fig. 6), although some gradients may exist along their lengths due to local dilution effects if the neuronal activity is also different in the different layers. Finally, large vessels are located on the cortical surface and should significantly contribute to stimulus-invoked signal changes in layer I in GE-BOLD maps and, to a much lesser extent, in the HSE-BOLD functional maps, as experimentally observed.

MION-based CBV maps display insensitivity to surface vessels, and the largest stimulus-evoked signal changes in the functional maps are in the middle layers. It is well known that CBV changes occur in all different size blood vessels. However, intravascular contrast agents such as MION can provide a filter against large vessels at sufficiently high concentrations because the presence of MION particles significantly suppresses baseline

intravascular signals from large vessels. Furthermore, the stimulus-evoked MION signal changes have a negative sign and thus are opposed by the positive BOLD contributions (Lu et al., 2004; Mandeville et al., 2004).

In view of the high capillary density in layer IV (Pawlik et al., 1981; Tieman et al., 2004), it can be argued that our observation of larger BOLD fMRI signal changes centered over layer IV reflect the larger basal blood volume in the middle layers at a constant stimulus-evoked blood flow and metabolic changes across the lamina. Similarly, a stimulus-evoked fractional CBV change that is constant across the layers can translate into a larger absolute CBV perturbation in the middle layers due to the higher basal capillary volume in this region and hence yield higher CBV-based fMRI signals in the middle layers. However, several observations argue against this as the only possibility: first, capillary density is well correlated with metabolic demand (Borowsky and Collins, 1989), and it is highly unlikely to invoke a situation where capillary density and energy demand are separable. Second, in cat area 18, layer IV contains the most active neurons as well as the highest stimulus-invoked glucose consumption (Vanduffel et al., 1995). Third, similarly high densities of capillaries are found in layers IV across areas 17 and 18 of the cat (Tieman et al., 2004), while the largest fMRI signals associated with the middle layers were observed mainly in area 18 (Fig. 6). As seen in Fig. 6, there is a sharp drop in the signal changes towards the transition zone and into area 17. If the signal changes were simply reflecting the vascular density in the different cortical layers, a more homogeneous distribution of signal changes would be expected across areas 17 and 18 in similar lamina. Therefore, we conclude that the layer-specific fMRI signals, neglecting the surface vessel effects, in both BOLD- and CBV-weighted images reflect translaminal inhomogeneities in stimulus-evoked metabolic demands and their corresponding vascular consequences.

As previously mentioned, CBF changes induced by altered neuronal activity are thought to correlate better with increased LFP rather than spiking activity (Mathiesen et al., 1998). Similarly, BOLD signal changes, which predominantly reflect blood flow perturbations, are thought to represent LFPs (Logothetis et al., 2001). Since alterations in cerebral glucose consumption and CBF are well correlated (Fox et al., 1988), increased metabolic activity can also be predicted to be associated with LFP increases. The studies leading to these conclusions (Mathiesen et al., 1998; Logothetis et al., 2001) are solely based on the temporal properties of CBF and BOLD signals. Nevertheless, they have implications as to the spatial location of the fMRI signals across the lamina; they suggest that fMRI signals reflect the neuronal inputs and local processing in layer IV which is the principal layer for the geniculocortical input to the primary visual cortex (Peters and Payne, 1993). Therefore, layer IV should exhibit the highest fMRI signals which can be explained in terms of neuronal and/or metabolic activity. Consistent with this prediction, our results display largest fMRI signals in layer IV, except in the case of GE-BOLD signals where large vessel obfuscation is present. However, while the spatial localization of the fMRI signals shown here may indicate the origin of the response, the data cannot resolve as to what type of neuronal activity (input–output) is associated with these fMRI signals.

Of the three different approaches examined in this study, the current CBV result reveals not only high specificity to the site of neuronal activity but also superior CNR relative to BOLD measurements. These advantages should certainly be taken into account when high spatial and/or temporal fMRI studies are planned where SNR is a limiting factor. However, it should be noted that the laminar specificities of the CBV maps are broader than those of the BOLD signals over the middle layers; maximum CBV signal changes incorporate layer IV and deeper parts of layer III. The laminar specificity of these CBV-weighted fMRI maps may not arise exclusively as a result of intrinsic specificity of CBV response to neuronal stimulation. Other factors such as contrast agent dose, magnetic field (through the BOLD mechanism that opposes the contrast agent effect) and enhanced sensitivity to partial volume effects are all expected to be important in determining the extent of this specificity. Furthermore, such CBV-weighted contrast agent-based studies are restricted to animal models since, in the desired dose, they are not currently clinically approved for human use.

In conclusion, we have demonstrated that BOLD “tissue” fMRI signals are centered over layer IV where CBV-weighted (MION) signals, with superior CNR, peak at layer IV and deeper parts of layer III. Our results show that fMRI studies utilizing a GE-BOLD sequence, even at high magnetic field and at high spatial resolution, are heavily weighted by surface vessels. However, microvascular contributions are also detectable at this high field strength in both the GE- and HSE-BOLD signals. The results also demonstrate that fMRI can be used for high-resolution sub-millimeter studies using contrasts which are less susceptible to large vessel changes, such as HSE-BOLD- or CBV-weighted MION. As higher field magnets are becoming more available and signal contrasts (intrinsic and extrinsic) with improved specificity are being developed, one should expect higher degrees of spatial correlation between fMRI and the underlying neurophysiological activity.

Acknowledgments

The authors would like to thank Dr. Y. Zhang for helping with animal preparations and Dr. R. Galuske for aiding with histological procedures. We would like to also thank Dr. G. Ghose for helpful discussions and Drs. G. Adriany and P. Anderson for hardware support. This work was supported by an NIH grants R01MH70800-01, R21EB004460, NIH (NCRR) grant P41-RR008079 and the MIND institute. Instrument acquisition was in part funded by the Keck Foundation.

References

Bandettini, P.A., Jesmanowicz, A., Wong, E.C., Hyde, J.S., 1993. Processing strategies for time-course data sets in functional MRI of the human brain. Magn. Reson. Med. 30, 161–173.

Borowsky, I.W., Collins, R.C., 1989. Metabolic anatomy of brain: a comparison of regional capillary density, glucose metabolism, and enzyme activities. J. Comp. Neurol. 288, 401–413.

Boxerman, J.L., Hamberg, L.M., Rosen, B.R., Weisskoff, R.M., 1995. MR contrast due to intravascular magnetic susceptibility perturbations. Magn. Reson. Med. 34, 555–566.

Caesar, K., Thomsen, K., Lauritzen, M., 2003. Dissociation of spikes, synaptic activity, and activity-dependent increments in rat cerebellar blood flow by tonic synaptic inhibition. Proc. Natl. Acad. Sci. U. S. A. 100, 16000–16005.

Duong, T.Q., Silva, A.C., Lee, S.P., Kim, S.G., 2000. Functional MRI of calcium-dependent synaptic activity: cross correlation with CBF and BOLD measurements. Magn. Reson. Med. 43, 383–392.

Duong, T.Q., Kim, D.S., Ugurbil, K., Kim, S.G., 2001. Localized cerebral

blood flow response at submillimeter columnar resolution. Proc. Natl. Acad. Sci. U. S. A. 98, 10904–10909.
Duong, T.Q., Yacoub, E., Adriany, G., Hu, X., Ugurbil, K., Kim, S.G., 2003. Microvascular BOLD contribution at 4 and 7 T in the human brain: gradient-echo and spin-echo fMRI with suppression of blood effects. Magn. Reson. Med. 49, 1019–1027.
Fox, P.T., Raichle, M.E., Mintun, M.A., Dence, C., 1988. Nonoxidative glucose consumption during focal physiologic neural activity. Science 241, 462–464.
Haacke, E.M., Brown, R.W., Thomphson, M.R., Venkatesan, R., 1999. Magnetic Resonance Imaging: Physical Principles and Sequence Design. John Wiley and Sons, Inc, New York.
Harel, N., Lee, S.P., Nagaoka, T., Kim, D.S., Kim, S.G., 2002. Origin of negative blood oxygenation level-dependent fMRI signals. J. Cereb. Blood Flow Metab. 22, 908–917.
Harrison, R.V., Harel, N., Panesar, J., Mount, R.J., 2002. Blood capillary distribution correlates with hemodynamic-based functional imaging in cerebral cortex. Cereb. Cortex 12, 225–233.
Heeger, D.J., Huk, A.C., Geisler, W.S., Albrecht, D.G., 2000. Spikes versus BOLD: what does neuroimaging tell us about neuronal activity? Nat. Neurosci. 3, 631–633.
Kennan, R.P., Scanley, B.E., Innis, R.B., Gore, J.C., 1998. Physiological basis for BOLD MR signal changes due to neuronal stimulation: separation of blood volume and magnetic susceptibility effects. Magn. Reson. Med. 40, 840–846.
Kwong, K.K., Belliveau, J.W., Chesler, D.A., Goldberg, I.E., Weisskoff, R.M., Poncelet, B.P., Kennedy, D.N., Hoppel, B.E., Cohen, M.S., Turner, R., et al., 1992. Dynamic magnetic resonance imaging of human brain activity during primary sensory stimulation. Proc. Natl. Acad. Sci. U. S. A. 89, 5675–5679.
Logothetis, N.K., Pauls, J., Augath, M., Trinath, T., Oeltermann, A., 2001. Neurophysiological investigation of the basis of the fMRI signal. Nature 412, 150–157.
Lu, H., Patel, S., Luo, F., Li, S.J., Hillard, C.J., Ward, B.D., Hyde, J.S., 2004. Spatial correlations of laminar BOLD and CBV responses to rat whisker stimulation with neuronal activity localized by Fos expression. Magn. Reson. Med. 52, 1060–1068.
Mandeville, J.B., Marota, J.J., Kosofsky, B.E., Keltner, J.R., Weissleder, R., Rosen, B.R., Weisskoff, R.M., 1998. Dynamic functional imaging of relative cerebral blood volume during rat forepaw stimulation. Magn. Reson. Med. 39, 615–624.
Mandeville, J.B., Jenkins, B.G., Chen, Y.C., Choi, J.K., Kim, Y.R., Belen, D., Liu, C., Kosofsky, B.E., Marota, J.J., 2004. Exogenous contrast agent improves sensitivity of gradient-echo functional magnetic resonance imaging at 9.4 T. Magn. Reson. Med. 52, 1272–1281.
Mathiesen, C., Caesar, K., Akgoren, N., Lauritzen, M., 1998. Modification of activity-dependent increases of cerebral blood flow by excitatory synaptic activity and spikes in rat cerebellar cortex. J. Physiol. 512 (Pt. 2), 555–566.
Movshon, J.A., Thompson, I.D., Tolhurst, D.J., 1978. Spatial and temporal contrast sensitivity of neurones in areas 17 and 18 of the cat's visual cortex. J. Physiol. 283, 101–120.
O'Leary, J.L., 1941. The structure of area striate of the cat. J. Comp. Neurol. 75, 131–164.
Ogawa, S., Lee, T.M., Kay, A.R., Tank, D.W., 1990. Brain magnetic resonance imaging with contrast dependent on blood oxygenation. Proc. Natl. Acad. Sci. U. S. A. 87, 9868–9872.
Ogawa, S., Tank, D.W., Menon, R., Ellermann, J.M., Kim, S.G., Merkle, H., Ugurbil, K., 1992. Intrinsic signal changes accompanying sensory stimulation: functional brain mapping with magnetic resonance imaging. Proc. Natl. Acad. Sci. U. S. A. 89, 5951–5955.
Ogawa, S., Menon, R.S., Tank, D.W., Kim, S.G., Merkle, H., Ellermann, J.M., Ugurbil, K., 1993. Functional brain mapping by blood oxygenation level-dependent contrast magnetic resonance imaging. A comparison of signal characteristics with a biophysical model. Biophys. J. 64, 803–812.
Pawlik, G., Rackl, A., Bing, R.J., 1981. Quantitative capillary topography and blood flow in the cerebral cortex of cats: an in vivo microscopic study. Brain Res. 208, 35–58.
Payne, B.R., 1990. Representation of the ipsilateral visual field in the transition zone between areas 17 and 18 of the cat's cerebral cortex. Vis. Neurosci. 4, 445–474.
Peters, A., Payne, B.R., 1993. Numerical relationships between geniculocortical afferents and pyramidal cell modules in cat primary visual cortex. Cereb. Cortex 3, 69–78.
Ress, D., Backus, B.T., Heeger, D.J., 2000. Activity in primary visual cortex predicts performance in a visual detection task. Nat. Neurosci. 3, 940–945.
Schuz, A., Palm, G., 1989. Density of neurons and synapses in the cerebral cortex of the mouse. J. Comp. Neurol. 286, 442–455.
Strupp, J., 1996. Stimulate: a GUI based fMRI analysis software package. NeuroImage 3, S607.
Thulborn, K.R., Waterton, J.C., Matthews, P.M., Radda, G.K., 1982. Oxygenation dependence of the transverse relaxation time of water protons in whole blood at high field. Biochim. Biophys. Acta 714, 265–270.
Tieman, S.B., Mollers, S., Tieman, D.G., White, J., 2004. The blood supply of the cat's visual cortex and its postnatal development. Brain Res. 998, 100–112.
Ugurbil, K., Adriany, G., Andersen, P., Chen, W., Garwood, M., Gruetter, R., Henry, P.G., Kim, S.G., Lieu, H., Tkac, I., Vaughan, T., Van De Moortele, P.F., Yacoub, E., Zhu, X.H., 2003. Ultrahigh field magnetic resonance imaging and spectroscopy. Magn. Reson. Imaging 21, 1263–1281.
Vanduffel, W., Vandenbussche, E., Singer, W., Orban, G.A., 1995. Metabolic mapping of visual areas in the behaving cat: a [14C]2-deoxyglucose study. J. Comp. Neurol. 354, 161–180.
Yacoub, E., Shmuel, A., Pfeuffer, J., Van De Moortele, P.F., Adriany, G., Andersen, P., Vaughan, J.T., Merkle, H., Ugurbil, K., Hu, X., 2001. Imaging brain function in humans at 7 Tesla. Magn. Reson. Med. 45, 588–594.
Yacoub, E., Duong, T.Q., Van De Moortele, P.F., Lindquist, M., Adriany, G., Kim, S.G., Ugurbil, K., Hu, X., 2003. Spin-echo fMRI in humans using high spatial resolutions and high magnetic fields. Magn. Reson. Med. 49, 655–664.
Yacoub, E., Van De Moortele, P.F., Shmuel, A., Ugurbil, K., 2005. Signal and noise characteristics of Hahn SE and GE BOLD fMRI at 7 T in humans. NeuroImage 24, 738–750.